

# Tunable asymmetric mode conversion using the dark-mode of three-mode waveguide system

Joonsoo Kim,<sup>1</sup> Seung-Yeol Lee,<sup>1</sup> Yohan Lee,<sup>1</sup> Hwi Kim,<sup>2</sup> and ByoungHo Lee<sup>1,\*</sup>

<sup>1</sup>National Creative Research Center for Active Plasmonics Application Systems, Inter-University Semiconductor Research Center and School of Electrical Engineering, Seoul National University, Gwanak-Gu Gwanakro 1, Seoul 151-744, South Korea

<sup>2</sup>ICT Convergence Technology for Health & Safety and Department of Electronics and Information Engineering, Korea University, 2511 Sejong-ro, Sejong 339-700, South Korea

\*byoungho@snu.ac.kr

**Abstract:** A design scheme for low-reflection asymmetric mode conversion structure in three-mode waveguide system is proposed. By using a dark-mode of three-mode system, which can be interpreted in terms of destructive interference of transition amplitudes, the transmission characteristics for forward and backward directions can be designed separately. After explanation of the proposed design scheme, we demonstrate an example of asymmetric mode converter that consists of two gratings. The proposed scheme may be useful for the design of tunable asymmetric transmission devices due to its design flexibility and efficient design process.

©2014 Optical Society of America

**OCIS codes:** (030.1670) Coherent optical effects; (050.2770) Gratings; (130.3120) Integrated optics devices; (230.7390) Waveguides, planar.

---

## References and links

1. L. Feng, M. Ayache, J. Huang, Y.-L. Xu, M.-H. Lu, Y.-F. Chen, Y. Fainman, and A. Scherer, "Nonreciprocal light propagation in a silicon photonic circuit," *Science* **333**(6043), 729–733 (2011).
2. L. Feng, Y.-L. Xu, W. S. Fegadolli, M.-H. Lu, J. E. B. Oliveira, V. R. Almeida, Y.-F. Chen, and A. Scherer, "Experimental demonstration of a unidirectional reflectionless parity-time metamaterial at optical frequencies," *Nat. Mater.* **12**(2), 108–113 (2012).
3. S. Fan, R. Baets, A. Petrov, Z. Yu, J. D. Joannopoulos, W. Freude, A. Melloni, M. Popović, M. Vanwolleghem, D. Jalas, M. Eich, M. Krause, H. Renner, E. Brinkmeyer, and C. R. Doerr, "Comment on Nonreciprocal light propagation in a silicon photonic circuit," *Science* **335**(6064), 38 (2012).
4. L. Feng, M. Ayache, J. Huang, and Y.-L. Xu, "Response to comments on Nonreciprocal light propagation in a silicon photonic circuit," *Science* **335**(6064), 38 (2012).
5. V. A. Fedotov, P. L. Mladyonov, S. L. Prosvirnin, A. V. Rogacheva, Y. Chen, and N. I. Zheludev, "Asymmetric propagation of electromagnetic waves through a planar chiral structure," *Phys. Rev. Lett.* **97**(16), 167401 (2006).
6. A. S. Schwanecke, V. A. Fedotov, V. V. Khardikov, S. L. Prosvirnin, Y. Chen, and N. I. Zheludev, "Nanostructured metal film with asymmetric optical transmission," *Nano Lett.* **8**(9), 2940–2943 (2008).
7. R. Singh, E. Plum, C. Menzel, C. Rockstuhl, A. K. Azad, R. A. Cheville, F. Lederer, W. Zhang, and N. I. Zheludev, "Terahertz metamaterial with asymmetric transmission," *Phys. Rev. B* **80**(15), 153104 (2009).
8. C. Menzel, C. Helgert, C. Rockstuhl, E.-B. Kley, A. Tünnermann, T. Pertsch, and F. Lederer, "Asymmetric transmission of linearly polarized light at optical metamaterials," *Phys. Rev. Lett.* **104**(25), 253902 (2010).
9. M. Mutlu, A. E. Akosman, A. E. Serebryannikov, and E. Ozbay, "Asymmetric transmission of linearly polarized waves and polarization angle dependent wave rotation using a chiral metamaterial," *Opt. Express* **19**(15), 14290–14299 (2011).
10. M. Kang, J. Chen, H.-X. Cui, Y. Li, and H.-T. Wang, "Asymmetric transmission for linearly polarized electromagnetic radiation," *Opt. Express* **19**(9), 8347–8356 (2011).
11. E. Plum, V. A. Fedotov, and N. I. Zheludev, "Asymmetric transmission: a generic property of two-dimensional periodic patterns," *J. Opt.* **13**(2), 024006 (2011).
12. C. Huang, Y. Feng, J. Zhao, Z. Wang, and T. Jiang, "Asymmetric electromagnetic wave transmission of linear polarization via polarization conversion through chiral metamaterial structures," *Phys. Rev. B* **85**(19), 195131 (2012).
13. M. Mutlu, A. E. Akosman, A. E. Serebryannikov, and E. Ozbay, "Diodelike asymmetric transmission of linearly polarized waves using magnetoelectric coupling and electromagnetic wave tunneling," *Phys. Rev. Lett.* **108**(21), 213905 (2012).
14. J. Shi, X. Liu, S. Yu, T. Lv, Z. Zhu, H. F. Ma, and T. J. Cui, "Dual-band asymmetric transmission of linear polarization in bilayered chiral metamaterial," *Appl. Phys. Lett.* **102**(19), 191905 (2013).

15. C. Pfeiffer, C. Zhang, V. Ray, L. J. Guo, and A. Grbic, "High performance bianisotropic metasurfaces: asymmetric transmission of light," *Phys. Rev. Lett.* **113**(2), 023902 (2014).
16. S. Cakmakcayan, A. E. Serebryannikov, H. Caglayan, and E. Ozbay, "One-way transmission through the subwavelength slit in nonsymmetric metallic gratings," *Opt. Lett.* **35**(15), 2597–2599 (2010).
17. J. Xu, C. Cheng, M. Kang, J. Chen, Z. Zheng, Y.-X. Fan, and H.-T. Wang, "Unidirectional optical transmission in dual-metal gratings in the absence of anisotropic and nonlinear materials," *Opt. Lett.* **36**(10), 1905–1907 (2011).
18. S. Cakmakcayan, H. Caglayan, A. E. Serebryannikov, and E. Ozbay, "Experimental validation of strong directional selectivity in nonsymmetric metallic gratings with a subwavelength slit," *Appl. Phys. Lett.* **98**(5), 051103 (2011).
19. E. Battal, T. A. Yogurt, and A. K. Okyay, "Ultrahigh contrast one-way optical transmission through a subwavelength slit," *Plasmonics* **8**(2), 509–513 (2013).
20. M. Stolarek, D. Yavorskiy, R. Kotyński, C. J. Zapata Rodríguez, J. Lusakowski, and T. Szoplik, "Asymmetric transmission of terahertz radiation through a double grating," *Opt. Lett.* **38**(6), 839–841 (2013).
21. Z. Cao, X. Qi, G. Zhang, and J. Bai, "Asymmetric light propagation in transverse separation modulated photonic lattices," *Opt. Lett.* **38**(17), 3212–3215 (2013).
22. A. E. Serebryannikov, E. Ozbay, and S. Nojima, "Asymmetric transmission of terahertz waves using polar dielectrics," *Opt. Express* **22**(3), 3075–3088 (2014).
23. T. Xu and H. J. Lezec, "Visible-frequency asymmetric transmission devices incorporating a hyperbolic metamaterial," *Nat. Commun.* **5**, 4141 (2014).
24. C. Lu, X. Hu, Y. Zhang, Z. Li, X. Xu, H. Yang, and Q. Gong, "Ultralow power all-optical diode in photonic crystal heterostructures with broken spatial inversion symmetry," *Appl. Phys. Lett.* **99**(5), 051107 (2011).
25. C. Wang, C.-Z. Zhou, and Z.-Y. Li, "On-chip optical diode based on silicon photonic crystal heterojunctions," *Opt. Express* **19**(27), 26948–26955 (2011).
26. C. Lu, X. Hu, H. Yang, and Q. Gong, "Ultrahigh-contrast and wideband nanoscale photonic crystal all-optical diode," *Opt. Lett.* **36**(23), 4668–4670 (2011).
27. H. Kurt, D. Yilmaz, A. E. Akosman, and E. Ozbay, "Asymmetric light propagation in chirped photonic crystal waveguides," *Opt. Express* **20**(18), 20635–20646 (2012).
28. V. Liu, D. A. B. Miller, and S. Fan, "Ultra-compact photonic crystal waveguide spatial mode converter and its connection to the optical diode effect," *Opt. Express* **20**(27), 28388–28397 (2012).
29. V. Kuzmiak and A. A. Maradudin, "Asymmetric transmission of surface plasmon polaritons," *Phys. Rev. A* **86**(4), 043805 (2012).
30. C. Wang, X.-L. Zhong, and Z.-Y. Li, "Linear and passive silicon optical isolator," *Sci. Rep.* **2**, 674 (2012).
31. A. Cicek and B. Ulug, "Coupling between opposite-parity modes in parallel photonic crystal waveguides and its application in unidirectional light transmission," *Appl. Phys. B* **113**(4), 619–626 (2013).
32. S. Feng and Y. Wang, "Unidirectional reciprocal wavelength filters based on the square-lattice photonic crystal structures with the rectangular defects," *Opt. Express* **21**(1), 220–228 (2013).
33. I. H. Giden, D. Yilmaz, M. Turduev, H. Kurt, E. Çolak, and E. Ozbay, "Theoretical and experimental investigations of asymmetric light transport in graded index photonic crystal waveguides," *Appl. Phys. Lett.* **104**(3), 031116 (2014).
34. A. E. Miroshnichenko, S. Flach, and Y. S. Kivshar, "Fano resonances in nanoscale structures," *Rev. Mod. Phys.* **82**(3), 2257–2298 (2010).
35. B. Luk'yanchuk, N. I. Zheludev, S. A. Maier, N. J. Halas, P. Nordlander, H. Giessen, and C. T. Chong, "The Fano resonance in plasmonic nanostructures and metamaterials," *Nat. Mater.* **9**(9), 707–715 (2010).
36. N. Papisimakis, V. A. Fedotov, N. I. Zheludev, and S. L. Prosvirnin, "Metamaterial analog of electromagnetically induced transparency," *Phys. Rev. Lett.* **101**(25), 253903 (2008).
37. J. Gu, R. Singh, X. Liu, X. Zhang, Y. Ma, S. Zhang, S. A. Maier, Z. Tian, A. K. Azad, H.-T. Chen, A. J. Taylor, J. Han, and W. Zhang, "Active control of electromagnetically induced transparency analogue in terahertz metamaterials," *Nat Commun* **3**, 1151 (2012).
38. S. C. Rand, *Lectures on Light: Nonlinear and Quantum Optics Using the Density Matrix* (Oxford University Press, 2010).
39. H.-C. Liu and A. Yariv, "Grating induced transparency (GIT) and the dark mode in optical waveguides," *Opt. Express* **17**(14), 11710–11718 (2009).
40. K. Xia, M. Alamri, and M. S. Zubairy, "Ultrabroadband nonreciprocal transverse energy flow of light in linear passive photonic circuits," *Opt. Express* **21**(22), 25619–25631 (2013).
41. H. Kim, J. Park, and B. Lee, *Fourier Modal Method and Its Applications in Computational Nanophotonics* (CRC Press, 2012).
42. A. Yariv, "Couple-mode theory for guided-wave optics," *IEEE J. Quantum Electron.* **9**(9), 919–933 (1973).
43. H. A. Haus and W. Huang, "Coupled-mode theory," *Proc. IEEE* **79**(10), 1505–1518 (1991).

## 1. Introduction

Photonic devices with asymmetric transmission characteristics have been considered for the realization of various functionalities in optical systems including optical isolation. For the cases of linear, passive, and non-magnetic systems, the Lorentz reciprocity condition poses a restriction on scattering matrices of the systems and only limited class of asymmetric transmission characteristics is allowed. Hence, the studies on asymmetric transmission in

linear, passive systems have been focused on asymmetric mode conversion that does not violate the Lorentz reciprocity [1–33]. For example, Feng et al. experimentally demonstrated asymmetric mode conversion on a silicon photonics platform using a complex modulation of permittivity and related their results to parity-time (PT) symmetry [1–4]. For circularly or linearly polarized light incidence, asymmetric transmission characteristics through two-layered or multi-layered chiral metamaterials were verified experimentally both in microwave and optical frequencies [5–16]. Asymmetric configurations of periodic structures were also shown to exhibit asymmetric transmission/reflection characteristics and one-way optical transmission characteristics were demonstrated [17–23]. For photonic crystal based structures, there were a number of successful demonstrations of one-way power transmission [25–33]. However, general strategies to obtain desired transmission characteristics are not extensively explored yet. In most cases, main focus was characterization of asymmetric transmission devices or design of optical diode operation. Actually, design of asymmetric transmission characteristics is challenging because simultaneous design of forward and backward propagation cases is required.

On the other hand, photonic analogues of atomic tri-level interference phenomena have attracted interest for several years. Especially, there have been numerous reports on photonic analogues of electromagnetically induced transparency (EIT) and Fano resonance using coupled resonators [34–37]. Though tri-level interference phenomena are mostly known for sharp spectral response that enables slow light, tri-level interference also introduces an interesting state of atom which is called the ‘dark state’ [38]. The dark state arises when two transitions induced by two coherent external fields destructively interfere. As a result of destructive interference, an atom at the dark state does not emit or absorb photon even at the presence of external field. In systems of weak gratings in waveguides, dark state has its photonic counterpart which is called the ‘dark-mode’ [39]. Just like dark state, mode transitions inside gratings are prohibited for dark-mode due to the destructive interference; the dark-mode remains stationary as a consequence. Regarding asymmetric transmission, Xia et al. already showed that broadband asymmetric transmission characteristics can be observed in a system of three coupled waveguides and interpreted their results in terms of coherent population trapping [40]. However, design strategy for forward/backward transmission characteristics was not discussed. We will show that the stationary property of the dark-mode can significantly lower the design complexity of asymmetric transmission devices by enabling separate design of forward and backward transmission characteristics.

In this paper, we propose a scheme for designing low-reflection asymmetric transmission structure in three-mode system. The proposed scheme exploits the dark-mode of the three-mode system, which will be explained in the next section. First, we designed a three-mode system that consists of two waveguides: one of which possesses the symmetric and anti-symmetric transverse electric (TE) mode (waveguide I) and the other one only supports the symmetric TE mode (waveguide II). Next, a grating for the two simultaneous mode coupling between the anti-symmetric TE mode of waveguide I and the symmetric modes of waveguides I and II was designed and the condition for the dark-mode of the three-mode system was specified. Then, we designed another grating that converts input mode to the specified dark-mode. Lastly, the asymmetric transmission characteristic of the cascade of two designed gratings is investigated. For full-field electromagnetic numerical calculation, Fourier modal method (FMM) is used for the excitation of input modes, the calculation of modal power flow, and the visualization of field distribution [41]. Although the design example presented in the following chapters is a two dimensional structure, the proposed scheme can also be applied to three dimensional waveguides. This is because the proposed scheme can be applied to any type of three waveguide modes that overlap each other regardless of the shape of waveguides.

## 2. Background theory and the proposed structure

In this section, the concept of the dark-mode in coupled mode theory (CMT) is briefly reviewed at first. Then, the configuration of asymmetric transmission device, which exploits a

property of the dark-mode of three-mode system, is proposed. A system of waveguides with weak perturbation can be described by the CMT [42, 43]. We start from a general form of CMT for three-mode system:

$$\begin{aligned}
ik_1 \frac{da_1}{dz} &= \mu_{12} a_2 e^{i\Delta_{12}z} + \mu_{13} a_3 e^{i\Delta_{13}z}, \\
ik_2 \frac{da_2}{dz} &= \mu_{12}^* a_1 e^{-i\Delta_{12}z} + \mu_{23} a_3 e^{i\Delta_{23}z}, \\
ik_3 \frac{da_3}{dz} &= \mu_{13}^* a_1 e^{-i\Delta_{13}z} + \mu_{23}^* a_2 e^{-i\Delta_{23}z},
\end{aligned} \tag{1}$$

where  $a_i, k_i$  are modal coefficients and propagation constants of  $i^{\text{th}}$  mode and  $\mu_{ij}$ ,  $\Delta_{ij} = k_j - k_i + q_{ij}$  are coupling coefficients and detuning parameters between  $i^{\text{th}}$  and  $j^{\text{th}}$  modes. For simplicity, it is assumed that the permittivity perturbation has the form of a cosine function. i.e.  $\Delta\mathcal{E}(x, y, z) = \sum_{i < j=1,2,3} \delta\mathcal{E}_{ij}(x, y) \cos(q_{ij}z)$ , and  $k_1 > k_2 > k_3$ . Now, we consider the case when there is no coupling between mode 1 and mode 3 and the condition  $\Delta_{12} = -\Delta_{23} = \Delta$  is satisfied. Then, Eq. (1) can be simplified to

$$i \frac{d}{dz} \begin{bmatrix} a_1 \\ a_2 \\ a_3 \end{bmatrix} = \begin{bmatrix} 0 & \mu_{12} e^{i\Delta z} / k_1 & 0 \\ \mu_{12}^* e^{-i\Delta z} / k_2 & 0 & \mu_{23} e^{-i\Delta z} / k_2 \\ 0 & \mu_{23}^* e^{i\Delta z} / k_3 & 0 \end{bmatrix} \begin{bmatrix} a_1 \\ a_2 \\ a_3 \end{bmatrix}. \tag{2}$$

When the amplitude ratio of mode is adjusted to  $[a_1 \ a_2 \ a_3]^T = [-\mu_{23} \ 0 \ \mu_{12}^*]^T$ , the right-hand side of the Eq. (2) vanishes. This means that the state is stationary despite there are couplings between modes. The cancellation of the right-hand side in the second line of Eq. (2) can be interpreted as a destructive interference between two transition amplitudes: one is a transition amplitude from the mode 1 to mode 2, and the other is one from the mode 3 to mode 2. This stationary state is known as the dark-mode in weak waveguide gratings [39]. Due to the resemblance of coupled mode equation and Schrödinger equation, direct analogy could be made in guided wave optics.

Now, we propose an example of asymmetric transmission structure taking advantage of the dark-mode. Figure 1(a) shows the schematic of the proposed device. A silicon waveguide (waveguide I) is designed to support both of the symmetric and anti-symmetric modes whereas the SiO<sub>2</sub> waveguide (waveguide II) can only support a symmetric mode. Waveguides are placed close enough to each other so that the waveguide modes can be coupled via gratings in the silicon waveguide. Throughout this paper, the mode 1, 2, and 3 refer to the symmetric mode of waveguide I, the anti-symmetric mode of waveguide I, and the symmetric mode of waveguide II, respectively. As depicted in Fig. 1(a), there are two cascaded waveguide gratings of different periods. The grating  $\alpha$  is perfectly tuned for the transition from mode 1 to mode 3. The grating  $\beta$ , which is tuned by the condition  $\Delta_{12} = -\Delta_{23} = \Delta$ , couples mode 2 with modes 1 and 3 simultaneously. Between the gratings  $\alpha$  and  $\beta$ , a spacing of length  $D$  is introduced for adjustment of relative phase between each mode as will be explained later.

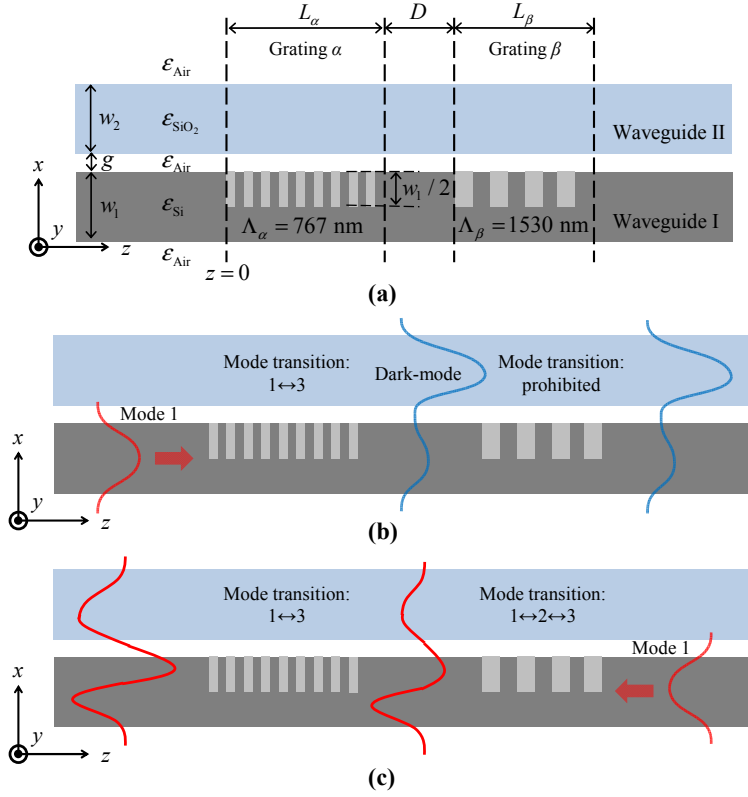


Fig. 1. (a) A schematic of the proposed device. A silicon waveguide ( $\epsilon_{\text{Si}} = 12.15$ ) of width  $w_1 = 400$  nm and a  $\text{SiO}_2$  waveguide ( $\epsilon_{\text{SiO}_2} = 2.25$ ) of width  $w_2 = 400$  nm are aligned in parallel with an air gap of width  $g = 100$  nm. The half-infinite areas above the waveguide II and beneath the waveguide I are set to air. (b) When mode 1 is incident from the left, the grating  $\alpha$  converts mode 1 to the dark-mode at the grating  $\beta$  and the dark-mode appears at the output because the dark-mode is stationary in the grating  $\beta$ . (c) When mode 1 is incident from the right, mode transitions in the grating  $\beta$  is not prohibited. As a result, various linear combinations of modes 1, 2 and 3 can appear at the output.

To observe left-to-right transmission characteristics, the mode 1 is launched from the left and enters the grating  $\alpha$ . Since the coupled mode equation for grating  $\alpha$  can be obtained by setting  $\mu_{12} = \mu_{23} = 0$ ,  $\mu_{13} = \mu_{13}^{(\alpha)}$  and  $\Delta_{12} = 0$  in Eq. (1), the coupled mode equation and its general solution can be derived as follows:

$$i \frac{d}{dz} \begin{bmatrix} a_1 \\ a_2 \\ a_3 \end{bmatrix} = \begin{bmatrix} 0 & 0 & \mu_{13}^{(\alpha)} / k_1 \\ 0 & 0 & 0 \\ \mu_{13}^{(\alpha)*} / k_3 & 0 & 0 \end{bmatrix} \begin{bmatrix} a_1 \\ a_2 \\ a_3 \end{bmatrix}, \quad (3)$$

$$\begin{aligned} a_1(z) &= a_1(0) \cos \Omega_{13}^{(\alpha)} z - i \sqrt{\frac{k_3 \mu_{13}^{(\alpha)}}{k_1 \mu_{13}^{(\alpha)*}}} a_3(0) \sin \Omega_{13}^{(\alpha)} z, \\ a_2(z) &= a_2(0), \\ a_3(z) &= a_3(0) \cos \Omega_{13}^{(\alpha)} z - i \sqrt{\frac{k_1 \mu_{13}^{(\alpha)*}}{k_3 \mu_{13}^{(\alpha)}}} a_1(0) \sin \Omega_{13}^{(\alpha)} z, \end{aligned} \quad (4)$$

where we define  $\Omega_{ij}^{(\zeta)2} = |\mu_{ij}^{(\zeta)}|^2 / k_i k_j$  ( $i < j = 1, 2, 3$  and  $\zeta = \alpha, \beta$ ). Here, we designed the length of grating  $\alpha$  ( $L_\alpha$ ) and the length  $D$  such that the following condition is satisfied:

$$\begin{bmatrix} \cos \Omega_{13}^{(\alpha)} L_\alpha \\ 0 \\ -i \sqrt{\mu_{13}^{(\alpha)*} k_1 / \mu_{13}^{(\alpha)} k_3} \sin \Omega_{13}^{(\alpha)} L_\alpha \end{bmatrix} = N \begin{bmatrix} \mu_{23}^{(\beta)} e^{-i2\pi(L_\alpha+D)/\Lambda_\beta} \\ 0 \\ -\mu_{12}^{(\beta)*} e^{i2\pi(L_\alpha+D)/\Lambda_\beta} \end{bmatrix}, \quad (5)$$

where  $N$  is a normalization constant and  $\mu_{12}^{(\beta)}, \mu_{23}^{(\beta)}$  are coupling coefficients of the grating  $\beta$ . Since the governing equation of the grating  $\beta$  is the Eq. (2), Eq. (5) implies that the dark-mode is formed at the entrance of the grating  $\beta$ . We note that the dark-mode expression on the right-hand side of Eq. (5) has an additional phase factor that represents the phase compensation due to the shift of grating position from the origin. Due to the fact that the dark-mode is stationary in region 2, the output on the right is the same as the left-hand side of Eq. (5).

On the other hand, when the mode 1 is launched from the right, the sequence of interaction is reversed. Unlike in the case of left-to-right propagation, the grating in region 2 induces modal transitions because the incident mode is not the dark-mode. The general solution for Eq. (2) is given by the following:

$$\begin{bmatrix} a_1 \\ a_2 e^{i\Delta z} \\ a_3 \end{bmatrix} = C_1 \begin{bmatrix} \mu_{23}^{(\beta)} \\ 0 \\ -\mu_{12}^{(\beta)*} \end{bmatrix} + C_2 \begin{bmatrix} \mu_{12}^{(\beta)} / k_1 \\ \Omega_- \\ \mu_{23}^{(\beta)*} / k_3 \end{bmatrix} \exp(-i\Omega_- z) + C_3 \begin{bmatrix} \mu_{12}^{(\beta)} / k_1 \\ -\Omega_+ \\ \mu_{23}^{(\beta)*} / k_3 \end{bmatrix} \exp(i\Omega_+ z),$$

$$C_1 = \frac{\mu_{23}^{(\beta)*}}{|\mu_{23}^{(\beta)}|^2 + k_3 |\mu_{12}^{(\beta)}|^2 / k_1} a_1(0) - \frac{\mu_{12}^{(\beta)}}{|\mu_{12}^{(\beta)}|^2 + k_1 |\mu_{23}^{(\beta)}|^2 / k_3} a_3(0), \quad (6)$$

$$C_2 = \frac{k_3 \mu_{12}^{(\beta)*}}{|\mu_{23}^{(\beta)}|^2 + k_3 |\mu_{12}^{(\beta)}|^2 / k_1} \frac{\Omega_+}{2\Omega} a_1(0) + \frac{1}{2\Omega} a_2(0) + \frac{k_1 \mu_{23}^{(\beta)}}{|\mu_{12}^{(\beta)}|^2 + k_1 |\mu_{23}^{(\beta)}|^2 / k_3} \frac{\Omega_+}{2\Omega} a_3(0),$$

$$C_3 = \frac{k_3 \mu_{12}^{(\beta)*}}{|\mu_{23}^{(\beta)}|^2 + k_3 |\mu_{12}^{(\beta)}|^2 / k_1} \frac{\Omega_-}{2\Omega} a_1(0) - \frac{1}{2\Omega} a_2(0) + \frac{k_1 \mu_{23}^{(\beta)}}{|\mu_{12}^{(\beta)}|^2 + k_1 |\mu_{23}^{(\beta)}|^2 / k_3} \frac{\Omega_-}{2\Omega} a_3(0),$$

where  $\Omega = \sqrt{\Omega_{12}^{(\beta)2} + \Omega_{23}^{(\beta)2} + \Delta^2 / 4}$  and  $\Omega_\pm = \Omega \pm \Delta / 2$ . Using Eqs. (4) and (6), it can be proved that the output for the right-to-left transmission case is:

$$|a_1| = \cos \Omega_{13}^{(\alpha)} L_\alpha,$$

$$|a_2| = \frac{k_3 |\mu_{12}^{(\beta)}|}{|\mu_{23}^{(\beta)}|^2 + k_3 |\mu_{12}^{(\beta)}|^2 / k_1} \left( \frac{\Omega_{12}^{(\beta)2} + \Omega_{23}^{(\beta)2}}{\Omega} \sin \Omega L_\beta \right). \quad (7)$$

We note that  $|a_1|^2$  is the same for left-to-right and right-to-left transmissions, which means consistency with Lorentz reciprocity and  $|a_3|^2$  can be determined by the energy conservation condition  $k_1 |a_1|^2 + k_2 |a_2|^2 + k_3 |a_3|^2 = k_1$ . The scenario of asymmetric mode conversion is summarized in the Figs. 1(b) and 1(c). As can be figured out from Eq. (5) and Eq. (7), the amplitudes of left-to-right transmission characteristic do not depend on  $L_\beta$  whereas those of right-to-left characteristic depend on  $L_\beta$ . Hence, it is possible to adjust  $|a_2|/|a_3|$  for right-to-left transmission without changing left-to-right transmission characteristics.

For clear understanding, we would like to summarize the design mechanism of the proposed asymmetric transmission structure. First, the ratio between coupling coefficients  $\mu_{23}^{(\beta)}$  and  $\mu_{12}^{(\beta)}$  of the grating  $\beta$  determines the dark-mode condition. Then, the period, length of grating  $\alpha$  and the value of  $D$  are determined to convert mode 1 to the dark-mode at the grating  $\beta$ . As a result, the output for the left-to-right transmission case is the dark-mode at the grating  $\beta$  regardless of  $L_\beta$  given that appropriate values for  $\Lambda_\alpha$ ,  $L_\alpha$  and  $D$  are chosen. After that, right-to-left transmission characteristics can be controlled by the value of  $L_\beta$ . The key advantage of the proposed structure is that the left-to-right transmission characteristics are not affected by the tuning of the right-to-left transmission characteristics. This observation implies that it is possible to design left-to-right and right-to-left transmission characteristics one by one. In the following sections, we demonstrate an example of asymmetric mode converter in detail.

### 3. Design of the grating $\beta$ and the specification of dark-mode

In order to define a dark-mode, a grating that makes two simultaneous couplings must be designed. Figure 2(a) shows the dispersion relation of the modes 1, 2 and 3. Since the dark-mode can exist only when the condition  $\Delta_{12} = -\Delta_{23}$  is satisfied, the period of the grating  $\beta$  should be tuned at  $4\pi/(k_1 - k_3)$ . At the same time,  $|\Delta_{12}| = |\Delta_{23}| = |\Delta|$  should be small compared to  $\sqrt{\Omega_{12}^{(\beta)2} + \Omega_{23}^{(\beta)2}}$  because, as can be predicted from Eq. (7), the accessible range of  $|a_2|$  for right-to-left transmission case decreases as  $|\Delta|$  increases. Hence, the widths of waveguides are adjusted so that propagation constants of three modes satisfy the condition  $k_1 - k_2 \approx k_2 - k_3$ . In our case, we chose  $w_1 = 400$  nm and  $w_2 = 400$  nm. The waveguides are designed at the freespace wavelength of 1550 nm and the gap width is set to 100 nm to retain coupling with the adjacent waveguide.

In order to check whether the grating is tuned, we consider a particular solution of Eq. (2) when  $a_2(0) = 1$  and  $a_1(0) = a_3(0) = 0$ :

$$\begin{bmatrix} a_1(z) \\ a_2(z) \\ a_3(z) \end{bmatrix} = \begin{bmatrix} -(i\mu_{12}^{(\beta)} / k_1\Omega)e^{i\Delta z/2} \cos \Omega z \\ e^{-i\Delta z/2} \cos \Omega z + i(\Delta / 2\Omega)e^{-i\Delta z/2} \sin \Omega z \\ -(i\mu_{23}^{(\beta)*} / k_3\Omega)e^{i\Delta z/2} \cos \Omega z \end{bmatrix}. \quad (8)$$

This particular solution implies in-phase modal coefficient oscillation of modes 1 and 3. When the grating is not tuned, one can expect the oscillation pattern would be distorted. For coupling of three modes, a binary grating inside the waveguide I is used. Though we used cosine permittivity modulation in our theoretical framework, the analysis in section 2 is still valid since the binary and cosine gratings of the same period are almost equivalent except that relatively weak higher order transitions may occur for binary gratings [42]. The grating occupies the half of the waveguide I to maximize coupling coefficients which are proportional to mode overlap integral [42]. The permittivity difference ( $\Delta\epsilon$ ) and the fill factor of the binary grating are set to  $-1$  and  $0.5$ , respectively, but we note that it is possible to choose other values given that the grating can be considered as a weak grating. Figures 2(b)-2(e) show the modal population evolution along propagation direction and  $E_y$  field distributions when we launched mode 2 from the left. When  $\Lambda_\beta = 1530$  nm, the grating is tuned and in-phase oscillation of modes 1 and 3 can be clearly observed as expected in Eq. (8). On the other hand, when we set  $\Lambda_\beta = 1550$  nm, the in-phase oscillation pattern is severely distorted.

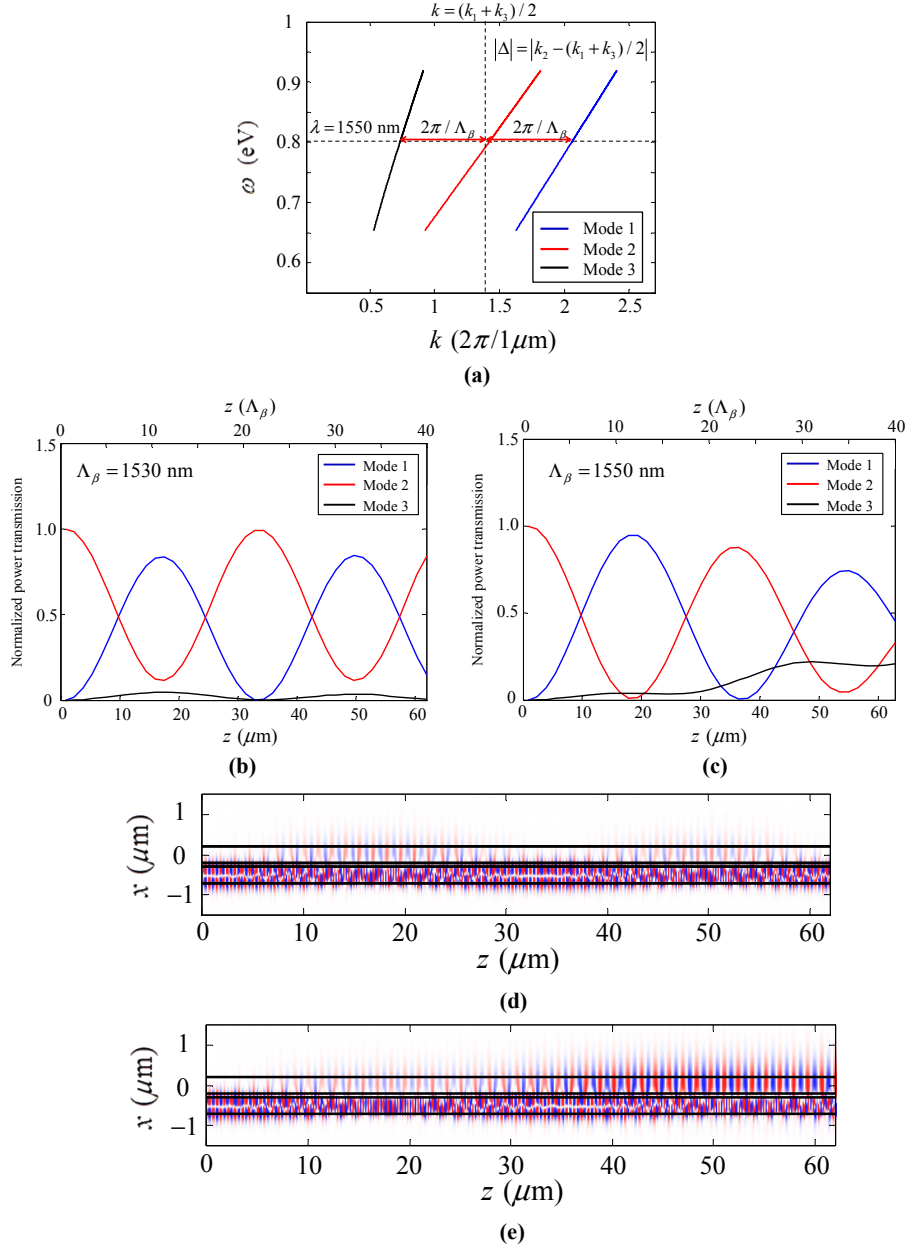


Fig. 2. (a) The dispersion relations of three modes considered in our configuration. The widths of two waveguide are adjusted so that  $\Delta k_{23} \approx \Delta k_{12}$  for simultaneous coupling of modes. Normalized power flow inside the grating  $\beta$  when (b)  $\Lambda_\beta = 1530$  nm and (c)  $\Lambda_\beta = 1550$  nm. Electric field ( $E_y$ ) distribution inside the grating  $\beta$  when (d)  $\Lambda_\beta = 1530$  nm and (e)  $\Lambda_\beta = 1550$  nm. Mode 2 is launched from the left and the waveguide centered at  $x = 0$  is the waveguide II.

After tuning of the grating, the dark-mode condition should be specified. A parametric study has been done to find out that the power flow ratio for modes 1 and 3 should be 5:95 to form a dark-mode in the previously designed grating  $\beta$ . Figure 3(a) shows that the power flow

of modes 1 and 3 is almost constant within the grating  $\beta$  when the dark-mode condition is well-satisfied. Electric field distribution ( $E_y$ ) of the dark-mode shown in Fig. 3(b) indicates that the dark-mode is not affected by the grating  $\beta$ . The dependence on the variation of incident power flow ratio and relative phase is investigated in Figs. 3(c) and 3(d), respectively. Unlike the case of exact dark-mode incidence, the normalized power flow of mode 3 changes along the propagation within the grating  $\beta$  when the input amplitude ratio and relative phase between the modes 1 and 3 are changed from the dark-mode condition. These results show that the stationary state shown in Fig. 3(b) is only achievable under the exact dark-mode condition which implies the destructive interference of modal transition amplitudes from mode 1 to mode 2 and that from mode 3 to mode 2.

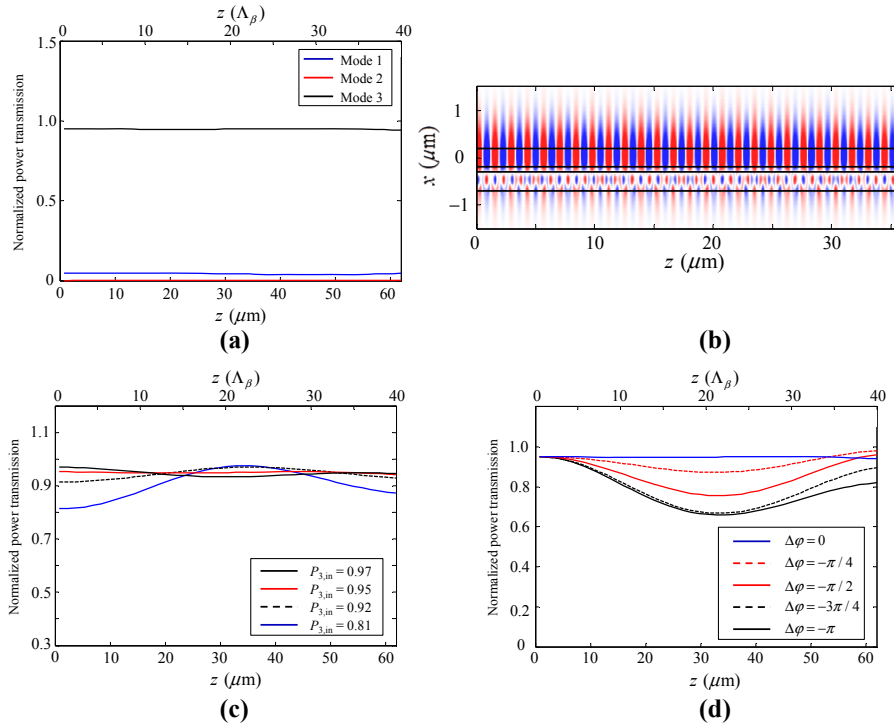


Fig. 3. (a) Normalized power flow in the grating  $\beta$  when the dark-mode is launched. (b)  $E_y$  field distribution of the dark-mode in the grating  $\beta$ . Normalized power flow of mode 3 in grating  $\beta$  when there is (c) a variation of normalized input power flow of mode 3 ( $P_{3,\text{in}}$ ) and (d) a variation of relative phase of mode 3 ( $\Delta\phi$ ) with respect to the exact dark-mode condition at the entrance of grating  $\beta$ .

#### 4. Dark-mode preparation and asymmetric transmission

Now, we focus on the design of grating  $\alpha$  of Fig. 1(a) which converts mode 1 to the dark-mode at the grating  $\beta$ . As we mentioned in section 2, the length of grating  $\alpha$  should be designed to match the modal population ratio of the dark-mode condition at the end of the grating. The transverse profile of the permittivity perturbation is the same as the grating  $\beta$ , but the grating period is set to 767 nm to couple modes 1 and 3. Figure 4(a) shows the normalized power flows inside the grating  $\alpha$  when the grating is exactly tuned for the transition from the mode 1 to mode 3. It was found that 67 periods are required for power flow ratio of 5:95 that we specified as the dark-mode condition. Next, the length  $D$  for relative phase adjustment should be determined, otherwise modal transitions occur in the grating  $\beta$  since the relative phase between the modes 1 and 3 at the entrance of grating  $\beta$  is also important for dark-mode condition. Figure 4(b) shows left-to-right transmission characteristics when only the

amplitude condition of the dark-mode in the grating  $\beta$  is satisfied, but a wrong value of  $D$  is chosen. Oscillation of power flows inside the grating  $\beta$  clearly shows that correct choice of  $D$  is critical for our design of asymmetric mode converter. To find the correct value of  $D$ , transmitted power flow at the end of the grating  $\beta$  is calculated for different values of  $D$  as shown in Fig. 4(c). Since  $L_\beta$  does not affect left-to-right transmission characteristic when the dark-mode condition is satisfied, the length of the grating  $\beta$  is temporarily set to 40 periods, which is long enough to clearly observe the stationary nature of the dark-mode. The value of  $D$  is changed from  $5 \mu\text{m}$  to  $5.75 \mu\text{m}$  since the period of beating for modes 1 and 3 is roughly  $750 \text{ nm}$ . As marked in Fig. 4(c), that transmitted power for mode 2 vanishes when  $D = 5.25 \mu\text{m}$  and the power flow ratio of modes 1 and 3 is roughly the same as the dark-mode. Figure 4(d) shows the modal power flows through two cascaded gratings for well-designed values of  $\Lambda_\alpha$ ,  $L_\alpha$ , and  $D$ ; it is clearly shown that modal power flows do not fluctuate in the grating  $\beta$ , which means that the dark-mode is incident on the grating  $\beta$  as we intended.

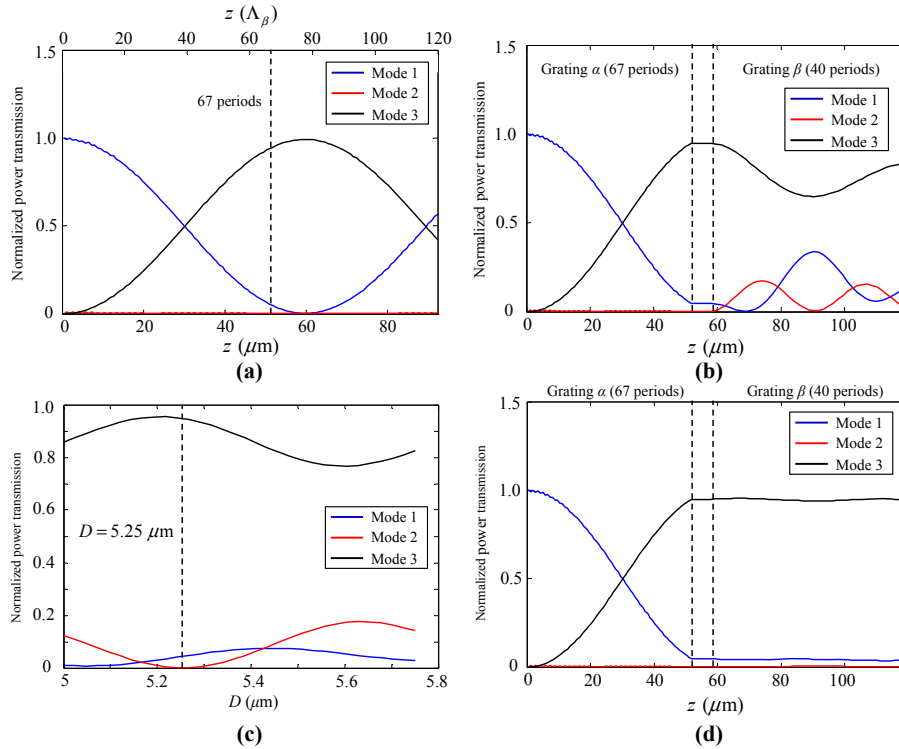


Fig. 4. (a) Normalized power flow inside the grating  $\alpha$  tuned for the transition from modes 1 to 3. (b) Normalized power flow through two cascaded gratings when a wrong value of  $D$  is chosen ( $D = 5.6 \mu\text{m}$ ). (c) Normalized power transmission after the two cascaded gratings depending on  $D$ . The length of the grating  $\beta$  is 40 periods. (d) Normalized power flow inside two cascaded gratings when  $D = 5.25 \mu\text{m}$ .

Now, let us consider the case of right-to-left transmission. As the length of the grating  $\beta$  does not affect left-to-right transmission characteristic for dark-mode incidence, it is possible to change right-to-left characteristics without changing left-to-right characteristics by adjusting  $L_\beta$ . Here, we recall that the grating  $\alpha$  is not tuned neither for the transition from mode 2 to mode 1 nor one from mode 2 to mode 3. Hence, when we neglect these transitions, the output power flow of the mode 2 for the right-to-left transmission case is not changed from the power flow of the mode 2 at the exit of the grating  $\beta$ . The power flow inside the two cascaded gratings that we designed to obtain Fig. 4(d) is shown in Fig. 5(a) for right-to-left propagation case. It can be observed that the power flow of the mode 2 does not change

significantly in the grating  $\alpha$  as we predicted. To determine the output power for the mode 2, modal energy transfer inside the grating  $\beta$  is investigated for mode 1 incidence as shown in Fig. 5(b). Depending on the value of  $L_\beta$ , the normalized power flow of the mode 2 can be tuned from 0 to 0.84. Therefore, it is possible to access wide range of right-to-left transmission characteristics. For clear demonstration of adjustable asymmetric transmission characteristics, we compared two cases in which the length of the grating  $\beta$  is set to 11 and 16 periods in Figs. 5(c)-5(f).

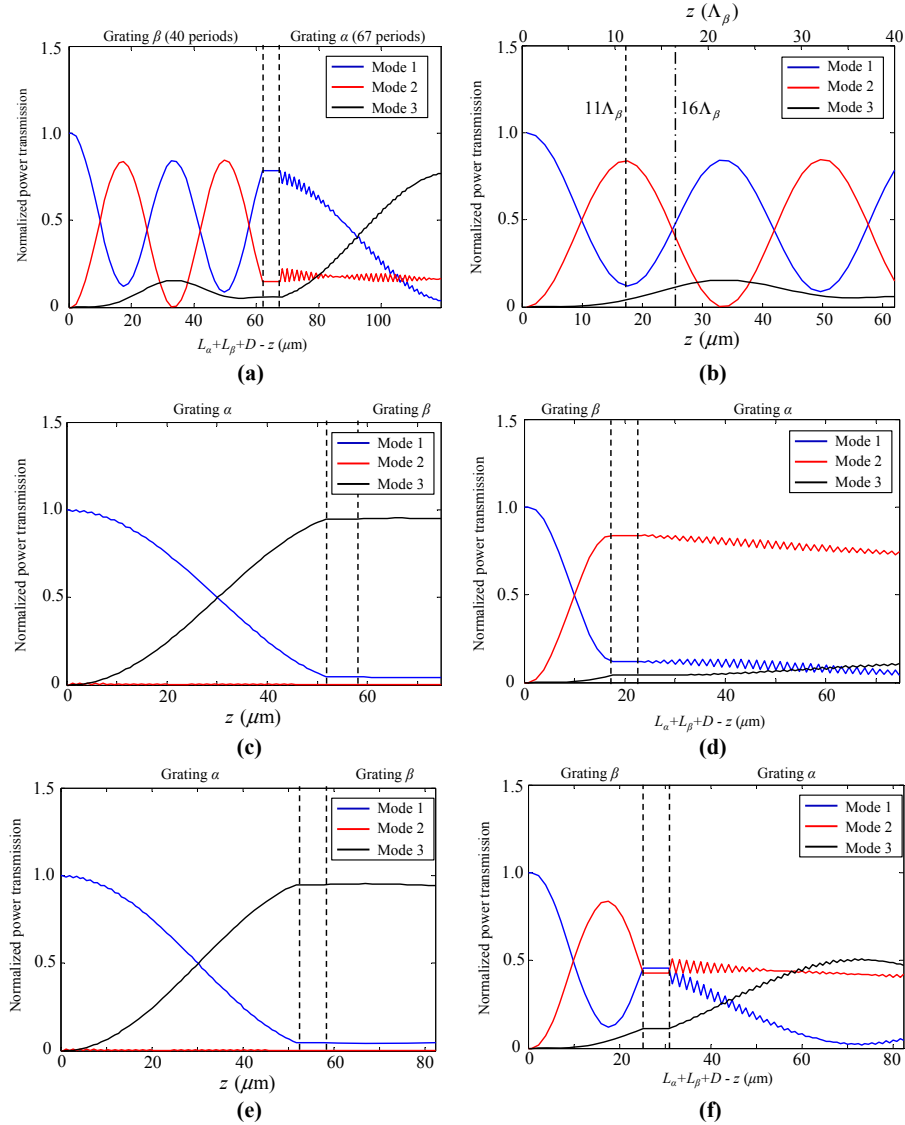


Fig. 5. (a) Normalized power flows inside the cascaded grating when the length of the grating  $\beta$  is set to 40 periods for the right-to-left propagation case. (b) Normalized power flows inside the grating  $\beta$  for the case of mode 1 incidence. Normalized power flows inside the cascaded gratings when the length of the grating  $\beta$  is set to 11 periods (c) for the left-to-right and (d) right-to-left propagation cases. (e) and (f) are those for the left-to-right and right-to-left propagation when the length of the grating  $\beta$  is set to 16 periods.

Figures 5(c)-5(d) and Figs. 6(a)-6(b) show the power flow dynamics and  $E_y$  field distributions for left-to-right and right-to-left propagation when the length of grating  $\beta$  is set

to 11 periods, whereas Figs. 5(e)-5(f) and Figs. 6(c)-6(d) show those when the length of grating  $\beta$  is set to 16 periods. When  $L_\beta$  is altered, the left-to-right transmission does not change as shown in Figs. 5(c) and 5(e) and the transmitted field distribution for left-to-right propagation depicted in Figs. 6(a) and 6(c) is that of the dark-mode. On the other hand, for right-to-left transmission as shown in Figs. 5(d) and 5(f), the output power flow ratio of modes 2 and 3 is changed as  $L_\beta$  increases. Hence, the asymmetric transmission characteristics in both directions are successfully designed. We note that the slight energy loss ( $< 1.2$  dB) is due to the leakage.

Before we conclude, some remarks must be made regarding small power flow oscillation of the modes 1 and 2 in the grating  $\alpha$ . This oscillation is due to the coupling of modes 1 and 2 which cannot be completely neglected, though the grating  $\alpha$  is severely detuned with respect to the transition between the modes 1 and 2. The reason why the amplitude of small oscillation varies by cases in Fig. 5 is because the oscillation amplitude depends on the ratio of modal coefficients which is  $a_2 / a_1$  in our case. For simple illustration of this effect, we consider a two level system which is described by the following coupled equations:

$$\begin{aligned}\frac{da_1}{dz} &= i \frac{\Omega}{2} a_2 e^{i\Delta z}, \\ \frac{da_2}{dz} &= i \frac{\Omega}{2} a_1 e^{-i\Delta z},\end{aligned}\quad (9)$$

where  $\Omega$  and  $\Delta$  represent coupling strength and detuning, respectively. When we set  $a_2(0) = \kappa a_1(0)$ , the Eq. (9) can be solved to obtain the following:

$$|a_1(z)|^2 = \left( \frac{1 + (\kappa\Omega - \Delta)^2}{2} - \frac{(\kappa^2 - 1)\Omega^2 - 2\Delta\kappa\Omega}{2(\Omega^2 + \Delta^2)} \cos(\sqrt{\Omega^2 + \Delta^2} z) \right) |a_1(0)|^2. \quad (10)$$

Hence, if  $\Omega \neq 0$ , oscillation amplitude depends on  $\kappa$ . More intuitive graphical explanation is possible using the Bloch's formulation of two level atoms which can be found in [38].

Now, we would like to conclude the section by briefly referring to the limitations of proposed design scheme. In principle, if the dispersion relations of three modes are carefully tuned so that  $\Delta = 0$  for the grating  $\beta$ , our design scheme enables design of arbitrary transmission characteristics in one direction, which was the right-to-left propagation case in our example. However, transmitted wave for the other propagation direction must be a dark-mode which is a linear combination of only two modes. Therefore, output power of one of three modes must be zero for one propagation direction. Moreover, our scheme itself does not provide a way to design transmission characteristics for every input mode or design of both transmission and reflection characteristics which is much more challenging. Another shortcoming of the proposed scheme is the long length of the device extending over several tens of  $\mu\text{m}$  due to the use of weak gratings. Therefore, development of compact mode converters is necessary for further improvements.

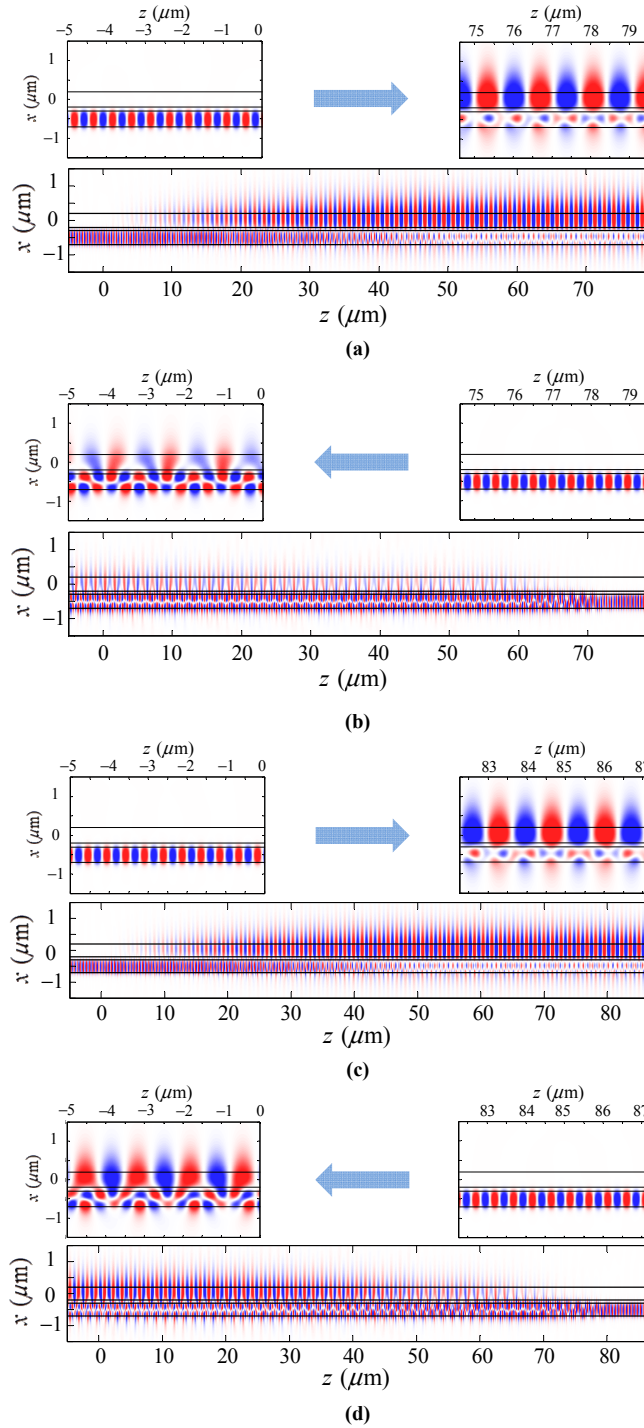


Fig. 6.  $E_y$  field distributions on two cascaded gratings for mode 1 incidence when the length of the grating  $\beta$  is set to 11 periods (a) for left-to-right and (b) right-to-left propagation cases. (c) and (d) are those when the length of the grating is set to 16 periods for left-to-right and right-to-left propagation cases, respectively. The field distributions of input and output are shown at the upper parts of each figure.

## 5. Conclusion

A scheme for designing asymmetric transmission devices in waveguide systems that support three modes is proposed. The proposed scheme exploits dark-mode which can be defined by a grating that couples one mode to two other modes simultaneously. Stationary property of the dark-mode fixes transmission characteristic in one direction, and it enables the independent design of transmission characteristics for left-to-right and right-to-left directions. Therefore, the scheme enables access to wide range of asymmetric transmission characteristics and the design process is purely sequential. Since the proposed scheme is applicable for various three-mode waveguide systems, asymmetric mode converters can be designed in different platforms following identical design process. Moreover, the design of active asymmetric transmission devices can be easier especially when it is required to tune the transmission characteristics in one direction and fix the transmission characteristics in the opposite direction. Therefore, the proposed scheme may find its applications in tunable, active asymmetric transmission devices.

## Acknowledgment

This work was supported by the National Research Foundation of Korea funded by Korean government (MSIP) through the Creative Research Initiatives Program (Active Plasmonics Application Systems).